



## Biocompatibility of the fiberoptic microneedle device chronically implanted in the rat brain

Yukitaka Kani<sup>a,b</sup>, Jonathan Hinckley<sup>a,b</sup>, John L. Robertson<sup>a,b</sup>, Jason M. Mehta<sup>a,b</sup>, Christopher G. Rylander<sup>a,b</sup>, John H. Rossmeisl<sup>a,b,\*</sup>

<sup>a</sup> *Veterinary and Comparative Neurooncology Laboratory and Animal Cancer Care and Research Center, Virginia-Maryland College of Veterinary Medicine, Virginia Tech, Blacksburg, VA, USA*

<sup>b</sup> *Department of Mechanical Engineering, University of Texas at Austin, Austin, TX, USA*

### ARTICLE INFO

#### Keywords:

Brain  
Convection enhanced delivery  
Fiberoptic microneedle device  
Neurotoxicology

### ABSTRACT

The fiberoptic microneedle device (FMD) is a fused-silica microcatheter capable of co-delivery of fluids and light that has been developed for convection-enhanced delivery and photothermal treatments of glioblastoma. Here we investigate the biocompatibility of FMD fragments chronically implanted in the rat brain in the context of evaluating potential mechanical device failure. Fischer rats underwent craniectomy procedures for sham control ( $n = 16$ ) or FMD implantation ( $n = 16$ ) within the brain. Rats were examined daily after implantation, and at 14, 30, 90, and 180 days after implantation were evaluated via computed tomography of the head, hematologic and blood biochemical profiling, and necropsy examinations. Clinical signs of illness and distant implant migration were not observed, and blood analyses were not different between control and FMD implanted groups at any time. Mild inflammatory and astrogliotic reactions localized to the treatment sites within the brain were observed in all groups, more robust in FMD implanted groups compared to controls at days 30 and 90, and decreased in severity over days 90–180 of the study. One rat developed a chronic, superficial surgical site pyogranuloma attributed to the FMD silica implant. Chronically implanted FMD fragments were well tolerated clinically and resulted in anticipated mild, localized brain tissue responses that were comparable with other implanted biomaterials in the brain.

### 1. Introduction

Convection-enhanced delivery (CED) is the continuous administration of a fluid containing therapeutic agent under positive pressure via stereotactically placed small-caliber catheter(s) inserted into the brain (Raghavan et al., 2006; Rossmeisl, 2017). The CED technique has been investigated for its potential usefulness for the treatment of brain tumors, because it allows the direct delivery of large molecule therapeutics to the tumor that would not normally pass through the blood brain barrier (BBB; Krauze et al., 2005, Rossmeisl et al., 2021, Ung et al., 2015). CED can also increase the distribution volume ( $V_d$ ) of the drug in the brain tissue orders of magnitude over what can be achieved by simple diffusion without significantly increasing intracranial pressure (Rossmeisl, 2017).

One of the major limitations of CED is the inability to consistently distribute therapeutic agents to the entire, biophysically heterogeneous, target brain or tumor volume (Mehta et al., 2017; Raghavan et al., 2006;

Rossmeisl et al., 2021). It has been shown that the  $V_d$  of CED infusates can vary depending on the tumor's location in the brain as well as its microenvironmental characteristics. For example, CED infusions performed in proximity to the ventricular system have a propensity to result in drug leakage into the low-pressure ventricles and drugs may pool in necrotic tumor regions preventing distribution to viable cancer cells (Mehta et al., 2017; Rossmeisl et al., 2021). Other major determinants of the efficacy of CED are physical features of the catheter. Historically, catheter clogging, infusate reflux or backflow, and air bubble formation have complicated complete treatment of brain tumors with CED (Mehta et al., 2017; Sampson et al., 2010). To overcome reflux, catheters have been designed to incorporate reflux-preventing properties such as a 'step change', in which the diameter of the catheter narrows the distal tip of the catheter (Krauze et al., 2005). These reflux preventing catheters have been shown to be capable of delivering CED infusates at high flow rates without reflux in humans and dogs with intracranial gliomas (Raghavan et al., 2006, Rossmeisl et al., 2021, Ung et al., 2015,

\* Corresponding author at: 205 Duckpond Drive, Virginia-Maryland College of Veterinary Medicine, Virginia Tech, Blacksburg, VA 24061, USA.  
E-mail address: [jrossmei@vt.edu](mailto:jrossmei@vt.edu) (J.H. Rossmeisl).

<https://doi.org/10.1016/j.rvsc.2021.12.018>

Received 27 September 2021; Accepted 28 December 2021

Available online 31 December 2021

0034-5288/© 2022 The Authors.

Published by Elsevier Ltd.

This is an open access article under the CC BY-NC-ND license

(<http://creativecommons.org/licenses/by-nc-nd/4.0/>).

Vogelbaum and Aghi, 2015).

Additional improvements to CED approaches for brain tumors have manifested as multiport catheters capable of delivering high volumes of therapeutics through a single insertion portal (Elenes et al., 2021; Vogelbaum et al., 2019). One example of such a multiport CED device is our proprietary arborizing catheter, the Convection Enhanced ThermoTherapy Catheter System (CETCS). The CETCS consists of a rigid primary cannula which contains up to seven ports, each of which houses an individual fiberoptic microneedle device (FMD; Fig. 1). Each FMD is a light-guiding, fused silica capillary tube capable of simultaneous co-delivering both fluids and light (Hood et al., 2013a; Hood et al., 2013b). The photothermal capabilities of the CETCS offer advantages over existing multiport CED catheter systems in that sublethal heating during infusion can increase the  $V_d$  of infusates by increasing fluid diffusion and convection, and reducing fluid viscosity (Hood et al., 2013a; Hood et al., 2013b). CETCS hyperthermic applications include laser interstitial thermoTherapy for tumor ablation, augmentation of the cytotoxicity of chemotherapeutic agents, or prevention of tumor cell seeding of needle track (Hood et al., 2013b; Liu et al., 2001; Saad and Hahn, 1992).

Possible adverse events associated with mechanical failure of the CETCS system would be breakage of a FMD deep within the brain parenchyma or subsequent migration of the broken FMD fragment outside of the brain. To evaluate the in vivo effects of these potential complications, the objectives of this study were to characterize the clinicopathologic responses to microneedle fragments chronically implanted in the brain of rats and determine if systemic FMD migration occurred in these rodents. We hypothesized that FMD fragments chronically implanted in the brain of rats would: 1) not cause clinical evidence of brain disease; 2) result in neuropathological findings similar to those observed with other chronically implanted catheters in the central nervous system (Butt, 2011); and 3) not migrate outside of the calvarium.

## 2. Materials and methods

### 2.1. Animals and study design

Thirty-two adult male Fisher rats were randomly assigned to sham control ( $n = 16$ ; FMD inserted into brain tissue and then withdrawn) and FMD implanted treatment groups ( $n = 16$ ; FMD fragment implanted within brain parenchyma). Surgical treatments were performed on study day 0. At 14, 30, 90 and 180 days following surgical treatments, 4 each of FMD implanted and sham control rats were weighed, had a complete

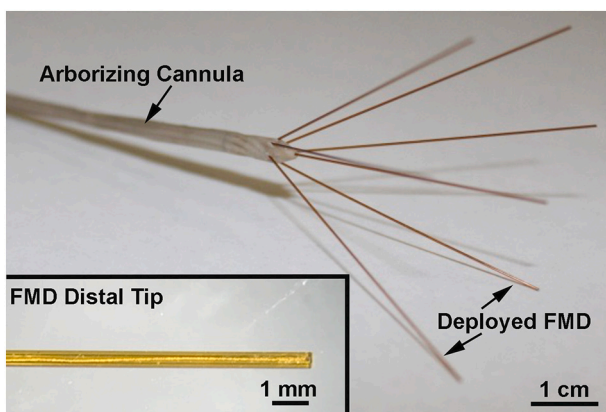


**Fig. 1.** The Convection Enhanced ThermoTherapy Catheter System (CETCS) consists of a primary arborizing cannula from which up to seven individual fiberoptic microneedle devices (FMD) can be deployed. Each FMD (inset) is constructed from small caliber fused-silica capillary tubing and capable of co-delivering fluids and light.

blood count and biochemical profile performed on peripheral blood and then were euthanized by barbiturate overdosage. A post-mortem micro-computed tomographic (mCT) imaging examination of the head and necropsy examination were then performed. The study was performed in accordance with the principles of Guide for the Care and Use of Laboratory Animals and was approved by the Institutional Animal Care and Use Committee of Virginia Tech (IACUC #19–245).

### 2.2. Craniectomy and FMD insertion into the brain

On day 0, the animals were weighed and premedicated with a 1.0 mg/kg subcutaneous injection of buprenorphine (SR-LAB; Zoopharm, Windsor, CO, USA), and then anesthetized with inhaled isoflurane (2–3.5%:95% isoflurane:oxygen mixture) delivered via nosecone. The dorsum of the head from the intercanthal area to the cranial cervical region was clipped and prepared for aseptic surgery. Anesthetized rats were placed in a small animal stereotactic headframe (Model 1350 M, David Kopf Instruments, Tungsten, CA, USA). A unilateral rostrotentorial surgical approach to the skull was performed and a 3 mm in diameter parietal craniectomy burr hole defect was created in the skull of each rodent using a high-speed electric drill. Randomly selected, sterile fragments of FMD (2–5 mm length; outer diameter = 365  $\mu\text{m}$ ; inner diameter = 150  $\mu\text{m}$ ) made from fused-silica capillary fibers (Fig. 1 inset; TSP180375, General Separation Technologies, Newark, DE, USA) were inserted through the burr hole, and implanted such that each fragment was completely embedded in the neuropil (Hood et al., 2013b). Following FMD implantation or sham treatment, the surgical incision was closed with tissue adhesive (VetBond, 3 M Animal Care Products, St. Paul, MN, USA).

### 2.3. Animal health status monitoring and euthanasia

Rats were housed in a temperature ( $26 \pm 1.5$  °C) and humidity controlled experimental room with a 12 h:12 h light-dark cycle in transparent polycarbonate cages, with 2 rats in each cage. Laboratory chow and water were provided ad libitum throughout the experiment. Rats underwent a 14 days acclimation period prior to the performance of the sham or FMD implantation surgery on day 0.

After craniectomy procedures, a health check was performed each day for the 180 days period of the study to examine signs of lassitude, social withdrawal, locomotion incoordination, dehydration, and surgical wound dehiscence or infection. The body weight of each animal was also recorded on the day of each of the predetermined survival endpoints, and animals were euthanized by intraperitoneal barbiturate overdosage (30 mg/kg Fatal Plus, Vortech Pharmaceuticals, Dearborn, MI, USA).

### 2.4. Hematological and biochemical analyses

For each rat, prior to the euthanasia, blood was collected via an intracardiac puncture and aliquoted into EDTA anti-coagulant and serum separator vacutainer tubes. Hemoglobin (Hb; %), hematocrit (Hct; %), mean corpuscular volume (MCV; fL), mean corpuscular hemoglobin (MCH; pg), red blood cell count (RBC;  $\times 10^6/\mu\text{L}$ ), total white blood cell count (WBC;  $\times 10^3/\mu\text{L}$ ), lymphocytes (%), monocytes (%), granulocytes (%) and platelets ( $\times 10^3/\mu\text{L}$ ) were determined using Sysmex XT-2000i analyzer (Sysmex, Mundelein, IL). Serum alanine transaminase (ALT; U/L), aspartate transaminase (AST; U/L), alkaline phosphatase (ALP; U/L), total bilirubin (mg/dL), albumin (g/dL), total protein (g/dL), cholesterol (mg/dL), glucose (mg/dL), blood urea nitrogen (mg/dL), and creatinine (mg/dL) were determined in serum with an AU400 analyzer (Olympus America, Center Valley, PA).

### 2.5. Micro-computed tomographic (mCT) imaging

Following euthanasia, each rat was decapitated and a mCT scan of

the head obtained (IVIS Spectrum CT, Perkin Elmer Caliper Life Sciences, Waltham, MA, USA) using the following acquisition parameters: voxel size = 75 μm, 50 kV, 1 mA, FOV: 6x6x3 cm to document the location of the FMD fragment in the brain. Decapitation was necessary because the mCT unit was designed to accommodate mice, and it was not possible to fit the body of an adult rat in the mCT gantry.

2.6. Necropsy, histopathology, and immunohistochemistry

Following euthanasia and mCT, a necropsy examination was performed on each rat. After immersion fixation in 10% neutral buffered formalin for 24 h, the extracted brain of each rat was mounted into a 2 mm matrix slicer (Zivic Instruments, Pittsburg, PA, USA) and sectioned in the transverse plane. Paraffin embedded tissues were sectioned at 5 μm and stained routinely with hematoxylin and eosin (H&E, Abcam, Cambridge, MA, USA). Histological slides of the brain stained with H&E were scored using a modification of previously reported grading system that accounts for brain and meningeal tissues responses to the presence of catheters in the nervous system (Table 1; Butt, 2011). Additional paraffin embedded, 3 μm brain sections were stained according to the manufacturer’s instructions with primary antisera against glial fibrillary acidic protein (GFAP; polyclonal, 1:150, Dako, Carpinteria, CA, USA), with an alkaline phosphatase detection method and fast red counterstain.

2.7. Statistical analyses

At each time point, unpaired *t*-tests were used to compare means of body weight, hematologic and biochemical variables, and histologic scores between sham control and FMD implanted groups, with significance defined as *p* < 0.05. All data were analyzed using Prism 9 software (version 9.2.0, GraphPad Software, San Diego, CA, USA).

3. Results

3.1. Animal health status

Clinical abnormalities were not observed in 14/16 sham controls or in 15/16 FMD implanted rats. Two sham control animals experienced surgical wound dehiscence in the first three days post-operatively, which were treated with primary wound closures with suture and subsequently resolved. One FMD implanted rat in the 180 day survival group developed a 5 mm in diameter, palpable subcutaneous soft-tissue swelling overlying the surgical site 126 days after the surgery, but this was not associated with other alterations in behavior. At the 180 day survival endpoint, this palpable swelling had increased in size to ~10 mm diameter. No differences in body weight (Fig. 2) were noted

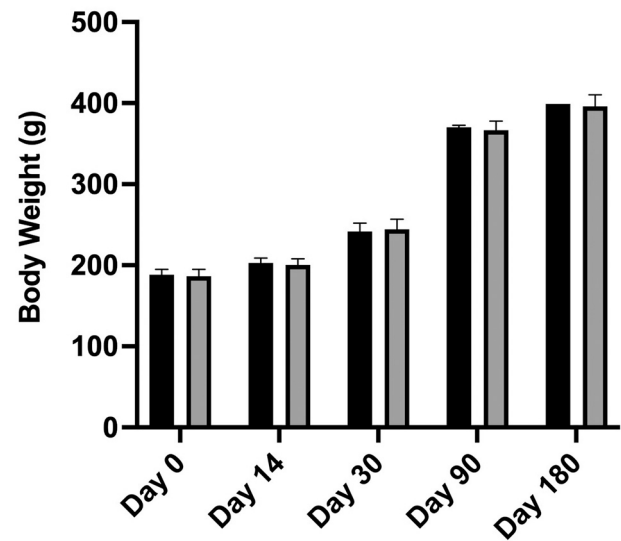


Fig. 2. Mean body weights of sham control (black) and FMD implanted rat (grey) groups over the study period.

between sham control or FMD implanted rats at any time point.

3.2. Hematologic and biochemical analyses

No differences in any hematologic or biochemical variables were observed between sham control and FMD implanted groups at any time point in the study (Table 2).

3.3. mCT imaging

Well margined craniectomy defects were clearly visible in all sham controls and 15/16 FMD implanted animals (Fig. 3). No imaging abnormalities within the brain were observed on mCT of any sham control rats. In 16/16 FMD implanted rats, the FMD fragment was visible on mCT as an intact well demarcated, linear hyperattenuating object within the brain parenchyma that was consistent with the size of the FMD implanted and in the location and trajectory of original implantation relative to the overlying craniectomy defect (Fig. 3B and C, arrows). No evidence of intracranial hemorrhage, air, or other brain lesions were observed on the mCT scans of FMD implanted rats. In the one FMD implanted rat in the 180 days survival group (rat 17) with the palpable cranial swelling (Fig. 3E and F, asterisk), soft tissue swelling and mineralization were observed on mCT in the area of the palpable swelling as well as expansile region of bone lysis associated with the

Table 1  
Histological grading system for evaluation of brain pathology in response to fiberoptic microneedle device implantation.

Severity	Absent	1	2	3	4	Severe
Response grade	0					5
Brain tissue response						
Mechanical lesion	No lesion	Surface contact or contusion	Needle track	Surface contact/contusion and needle track	Puncture of ventricle	Surface contact/contusion, needle track, and puncture of ventricle
Hemorrhage		Mild, focal	Mild, local to needle track	Regional, around needle track	Moderate	Severe
Inflammation/ edema		None	Mild, local to needle track	Regional, around needle track	Moderate	Severe
Parenchymal necrosis		Absent	Absent		Localized to needle tip	Regional necrosis around and remote from needle tip
Meningeal reaction						
Meningeal inflammatory infiltrate	No lesion	Local, mild	Local, moderate	Local, severe	Regional	Diffuse

The total histologic score = Brain tissue response grade + meningeal reaction grade.  
Modified from Butt (2011).

**Table 2**  
Hematologic and serum biochemical profiles by group and time.

Clinicopathologic parameter	Group1 (Day 14)			Group 2 (Day 30)			Group 3 (Day 90)			Group 4 (Day 180)		
	Sham		FMD implant	Sham		FMD implant	Sham		FMD implant	Sham		FMD implant
	Mean	SD	Mean	SD	Mean	SD	Mean	SD	Mean	SD	Mean	SD
Hemoglobin (mg/dl)	15.61	0.78	15.05	0.39	15.09	0.81	15.65	0.89	15.40	0.45	15.25	0.37
Hematocrit (Hct; %)	50.58	1.16	49.80	0.96	49.02	1.22	48.99	1.11	50.70	1.18	50.25	1.12
Mean Corpuscular Volume (MCV;fl)	61.19	1.06	61.42	1.29	61.25	0.51	61.88	0.39	61.33	0.46	61.21	1.02
Mean Corpuscular Hemoglobin (MCH; pg)	19.89	0.35	19.95	0.41	19.65	0.42	19.98	0.51	19.90	0.49	20.08	0.17
Red Blood Cells ( $\times 10^6/\mu\text{L}$ )	8.04	0.18	7.96	0.15	7.94	0.21	8.00	0.24	7.98	0.14	8.06	0.13
Total WBC ( $\times 10^6/\mu\text{L}$ )	8.15	0.84	8.66	0.29	7.93	1.23	8.34	0.70	8.55	0.80	9.77	3.14
Lymphocytes %	76.80	2.49	75.25	1.49	74.83	2.29	76.23	1.53	74.84	2.23	76.50	2.36
Monocytes %	3.08	0.26	3.15	0.21	3.18	0.14	3.33	0.33	3.21	0.17	3.15	0.21
Granulocytes%	18.31	1.12	19.85	0.79	17.58	1.74	18.83	0.64	18.29	1.08	19.90	2.02
Platelets ( $\times 10^3/\mu\text{L}$ )	783.53	31.67	772.75	28.65	777.84	26.82	793.50	19.64	781.06	32.66	799.00	38.93
Alanine Transaminase (ALT; U/L)	43.44	4.27	40.91	6.78	42.97	3.34	41.17	3.76	46.88	5.90	44.47	4.93
Aspartate Transaminase (AST; U/L)	132.87	9.95	138.46	5.74	143.23	10.48	138.62	8.53	146.61	11.17	141.19	13.92
Alkaline Phosphatase (ALP; U/L)	369.34	26.29	376.41	9.86	379.37	16.50	388.94	12.17	394.39	24.45	359.22	23.78
Total Bilirubin (mg/dl)	0.06	0.04	0.07	0.02	0.08	0.03	0.08	0.04	0.09	0.03	0.07	0.02
Albumin (g/dl)	3.91	0.24	3.95	0.13	3.96	0.21	3.85	0.19	3.94	0.20	3.83	0.21
Total Protein (g/dl)	6.27	0.29	6.15	0.21	6.28	0.22	6.35	0.13	6.19	0.32	6.18	0.19
Cholesterol (mg/dl)	74.26	11.61	72.64	7.14	74.85	9.39	71.06	7.75	73.35	10.94	74.62	8.49
Glucose (mg/dl)	79.27	8.66	81.75	5.32	84.36	7.57	80.00	5.60	82.25	4.65	79.50	7.55
Blood urea nitrogen (mg/dl)	15.21	2.46	16.03	1.63	16.77	3.06	18.25	2.22	16.56	2.38	16.17	1.59
Creatinine (mg/dl)	0.34	0.06	0.35	0.03	0.33	0.04	0.35	0.05	0.36	0.04	0.36	0.05

craniectomy defect.

### 3.4. Necropsy, histopathology, and immunohistochemistry

No gross lesions were observed in the brains of sham controls (Fig. 4A1). On gross examination of FMD implanted rats, focal meningeal exudates were observed on the dorsal surface of the cerebrum and were visible at the point where FMD fragments were inserted into brain in the day 14 and 30 (Fig. 4A2) groups. In the day 30 and 90 groups, punctate depressions on the dorsal aspect of the cerebrum were observed where FMD fragments were inserted into the brain. In some animals, the brain extraction procedure resulted in the proximal tip of the FMD fragment protruding into the center of these depressions (Fig. 4A3). Following transverse sectioning of the brain, implanted FMD fragments were clearly visible, but were not associated with grossly apparent lesions in the brain parenchyma (Fig. 4A4). FMD implanted rat 17 (180 day survival group) was the only animal with an observable gross lesion outside of the brain. This rat had a palpable soft-tissue swelling on the head, was noted to have an epidural abscess affecting the calvarium immediately adjacent to the craniectomy site extending into the overlying soft tissues.

Brain histological scores in FMD implanted rats were significantly higher than controls at days 30 and 90 (Fig. 4B). The severity of histologic brain lesions successively increased in both sham and FMD implanted groups over days 14–90 of the study, with very mild lesions present in sham control and FMD implanted rats by study day 180.

In sham controls, histologic lesions consisted of surface contusions and mild hemorrhage, edema, and mixed suppurative and mononuclear brain parenchymal and meningeal inflammatory infiltrates that were localized to catheter tracks or the craniectomy site on Day 14 (Fig. 4C1 and C4). On days 30 and 90, inflammatory infiltrates in the meninges and brain were predominantly mononuclear and contained hemosiderin laden macrophages (Fig. 4C7). Increased numbers and sizes of glial cells, which were confirmed to be predominantly astrocytes on GFAP immunohistochemistry, were noted adjacent to catheter tracks (Fig. 4C4). Sham control animals had minimal lesions consisting of scant gliosis along the catheter insertion tracks at day 180 (Fig. 4C10).

In FMD treated rats, observed meningeal infiltrates were similar in type but slightly more extensive than those observed in controls (Fig.4C2, C3, and C5) at the same time points. Brain parenchymal edema, inflammation, astrogliosis, and hemorrhage were also similar in morphology to controls but more severe in their regional extent of involvement of the brain surrounding the FMD implants (Fig. 4C2, C5, and C6). Brain parenchymal necrosis localized to distal tips of the FMD was also observed in treated rats at days 30 (Fig. 4C5) and 90 (Fig. 4C8 and C9). The predominant histological brain lesion in the day 180 FMD group was mild gliosis along the catheter implant tracks (Fig. 4C11, arrow). In the day 180 FMD implanted rats, one animal (rat 17) had a pyogranulomatous epidural mass, meningeal fibrosis, and calvarial osteomyelitis in the region of the craniectomy. Angular, refringent polarizing material was detected within the pyogranuloma, consistent with silica glass fragments (Fig. 4C12). Histologic changes were not observed in the brain parenchyma of rat 17.

Localized astrogliotic reactions, as evaluated with GFAP immunohistochemistry, adjacent to catheter tracks and catheter tips were noted in all groups at all time points. These were interpreted as minimal in the day 14 groups, mild in both 30 days groups, and subsequently decreased in severity at 90 and 180 days, with the extent of reaction in the 180 days groups resembling those seen in the day 14 groups (Fig. 4C). Astrogliotic reactions in FMD implanted rats resembled those of control rats in morphology, but extended further into the brain parenchyma surrounding the FMD implants.

## 4. Discussion

As the CETCS system was originally intended for single use, short

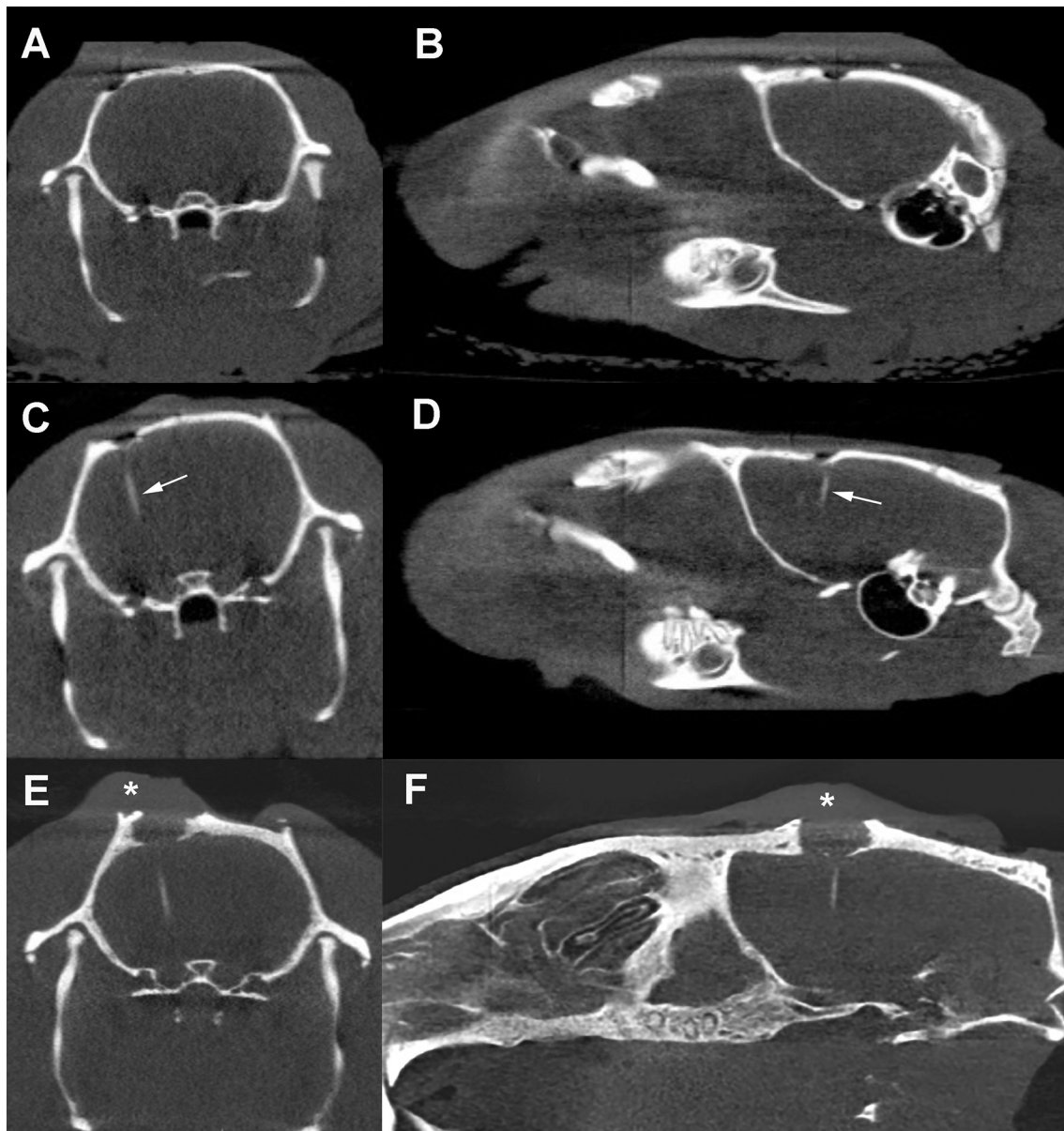


**Fig. 3.** Representative micro-computed tomographic scans of control (A, B) and FMD implanted (C–F) rats obtained at day 90, and from the one FMD implanted rat that developed a surgical site pyogranuloma and calvarial osteomyelitis (E, F) 180 days after treatment. The implanted FMD are visible as linear, hyperattenuating objects (arrows) within the brain parenchyma underlying the craniectomy defects. The soft tissue swelling (E, F asterisk) and expansile, osteolytic reaction in rat 17 are apparent.

duration interstitial delivery of infusates into the brain, this study was primarily conducted to evaluate the biological responses to mechanical device failure (Elenes et al., 2021; Hood et al., 2013a). However, given the advantages the photothermal capabilities of the FMD, we also envision the potential value of chronically implanting the device in the brain for long-term continuous or intermittent infusions or optogenetic therapies for neurodegenerative disorders (Montagni et al., 2019).

In rats with FMD chronically implanted in the brain, we did not observe evidence of neurologic or systemic constitutional illness, hematologic or biochemical alterations that were different than controls, or migration of the devices outside of the calvarium. The tissue reactions in the brain associated with the FMD consisted of hemorrhage, inflammation, and astroglia at the implant site, and were more locally robust than seen in controls.

Silica based medical devices and biomaterials have been developed and used for over 6 decades for numerous indications, but the major current medical use of silica implants is for bioactive glass applications

in bone healing, although fused silica and ceramic catheters have been used for CED applications in the brain (Barua et al., 2013; Hayn et al., 2017; Rossmeisl et al., 2021; Ung et al., 2015). The brain tissue responses we observed to the fused silica FMD fragments were similar in morphology, extent, and temporal evolution to other studies that have reported brain pathology associated with implanted catheters made of silica and other biomaterials (Butt, 2011; Hayn et al., 2017; Linsmeier et al., 2009; Rossmeisl et al., 2021; Zhong and Bellamkonda, 2008). In our study, the mechanical damage to the brain tissue and resulting inflammation were restricted to the implant sites, with the most severe lesions occurring around the tips of the devices, and these injury responses declined in severity between 3 and 6 months (Butt, 2011). A biocompatibility study of silicon oxide coated nanowires implanted in the rat brain evaluated local effects of the nanowires at 1, 6 and 12 weeks after implantation, and also observed increased glial responses in the first week, which declined over time (Linsmeier et al., 2009). This study also found evidence that the nanowires were able to cross the

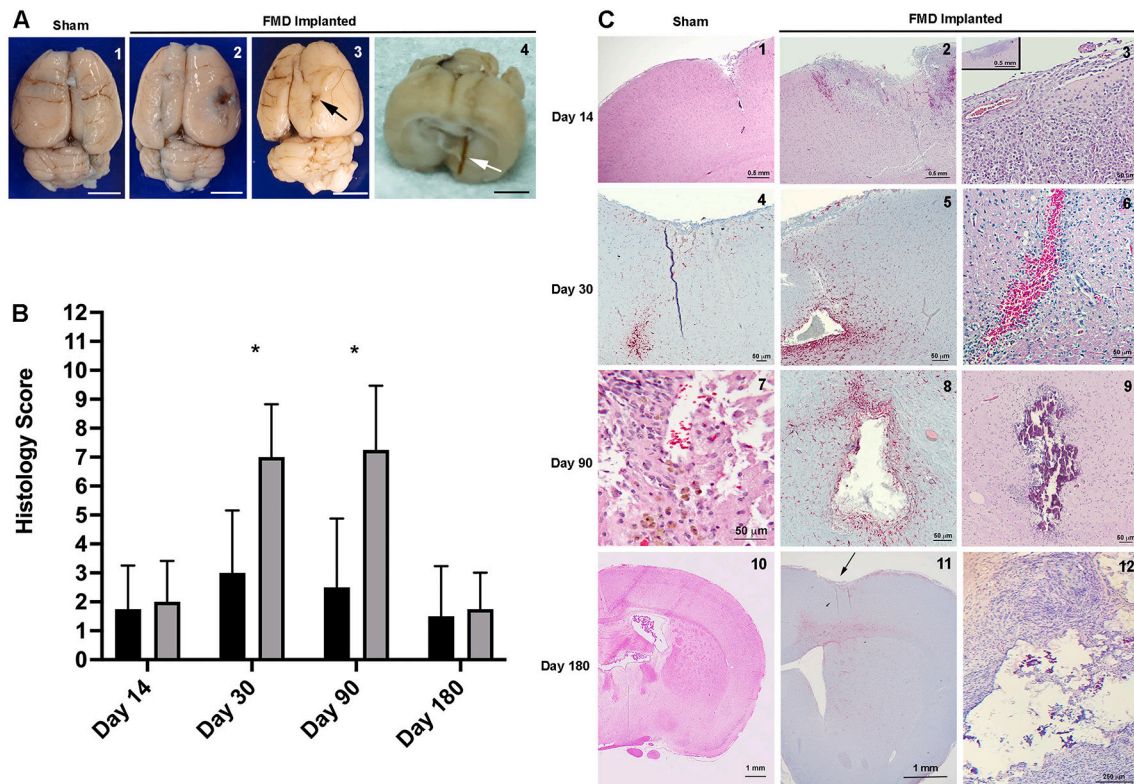


**Fig. 4.** Summary of neuropathological findings. A- Gross brain specimens were unremarkable in sham controls (1, day 14). In FMD implanted rats, focal meningeal exudates were visible on the brain surface at the implantation site on days 14 and 30 (2) in FMD implanted rats, and punctate depressions in the brain were seen at the implant site (3, day 90, arrow). FMD fragments were clearly visualized within the brain tissue upon sectioning, but were not associated with gross lesions (4, day 180, arrow). Bar = 3 mm in all panels. B- FMD implanted rats had significantly higher histologic scores than controls at days 30 (\*,  $p = 0.03$ ) and 90 (\*,  $p = 0.02$ ). C- Focal meningeal and brain parenchymal inflammatory infiltrates (1–7) and astrogliosis (4, 5, 8) are present surrounding the implantation site at days 14–90 and are more extensive in FMD implanted animals than controls. Brain necrosis at catheter tips (5, 8, 9) was visible in day 30 and 90 FMD implanted rats. Lesions were minimal in day 180 groups, and consisted of mild gliosis along the catheter track (10, 11, arrow). Angular, refractile silica fragments are visible among the pyogranulomatous reaction (12) observed in rat 17 at day 180. Panels 1–3, 6, 7, 9, 10, and 12, H&E stain. Panels 4, 5, 8, 11, GFAP immunohistochemistry.

blood brain barrier and leave the brain, and were partially degraded by microglia by weeks 6 and 12 (Linsmeier et al., 2009).

The FMD device can be clearly visualized with computed tomographic imaging, which is important to confirm its intended location for clinical indications in the brain, but also to monitor catheter placement and integrity when chronically implanted. Although we did not see any signs of distant FMD migration, this is likely because the size of the implanted fragment was too large to pass intact through the rat brain vessels. However, given the clinical, mCT, and histologic findings observed in the one FMD treated rodent in the 180 days survival group, we suspect that the proximal end of the FMD migrated locally through the meninges into the overlying soft-tissues and was damaged. The subsequent mechanical irritation and presence of the silica fragments subsequently led to the pyogranuloma and osteomyelitis at the surgical site, which is a clinical situation that clinically could have been mitigated with a relatively straightforward local debridement intervention. Given the robust and mixed osteoproliferative and osteolytic bone tissue response observed in the skull of this rat, we cannot completely exclude the possibility that the fused-silica FMD device has bioactive glass properties upon degradation (Henstock et al., 2015).

We have used both FMD and the CETCS system to perform CED and laser interstitial thermotherapy in the brain of multiple animal model systems without evidence of mechanical device failure (Elenes et al., 2021; Hood et al., 2013a; Hood et al., 2013b; Sharma et al., 2020). However, the observations in the rat with the pyogranuloma highlights the need to evaluate other modes of mechanical failure of the FMD device that simulate the presence and degradation profiles of pulverized silica microfragments within tissues over a more protracted period. This

design scenario would be appropriate to model biological and clinical effects of systemic biomaterial migration and intravascular object embolization.

## 5. Conclusions

Chronically implanted FMD fragments in the rat brain were well tolerated clinically, did not migrate distantly or cause significant systemic alterations, and resulted in anticipated mild, localized brain tissue responses that diminished in magnitude over the 6 months study period and were comparable with other implanted biomaterials in the brain. From this biocompatibility data and our clinical experience, we conclude that the risk-benefit profile of the CETCS device is favorable given its primary intended indication for single, short-term use in the treatment of malignant glioma.

## Author contributions

Christopher G. Rylander and John H. Rossmeisl contributed to the study conception and design. All authors participated in material preparation, data collection and data analysis. The first draft of the manuscript was written by Yukitaka Kani and all authors commented on previous versions of the manuscript. All authors read and approved the final manuscript.

## Declaration of Competing Interest

John L. Robertson, Christopher G. Rylander and John H. Rossmeisl

hold a patent (US20130338627A1) related to therapeutic applications of the fiberoptic microneedle device.

## Acknowledgements

This study was funded by grant P01CA207206 from the National Institutes of Health/National Cancer Institute.

## References

- Barua, N.U., Lewis, S.P., Woolley, M., O'Sullivan, S., Harrison, R., Gill, S.S., 2013. Robot-guided convection-enhanced delivery of carboplatin for advanced brainstem glioma. *Acta Neurochir.* 155, 1459–1465.
- Butt, M.T., 2011. Morphologic changes associated with intrathecal catheters for direct delivery to the central nervous system in preclinical studies. *Toxicol. Pathol.* 39, 213–219.
- Elenes, E.Y., Mehta, J.N., Hsu, F.-C., Whitlow, C.T., Debinski, W., Rossmeisl, J., Tatter, S., Rylander, C.G., 2021. Convection-enhanced arborizing catheter system improves local/regional delivery of infusates versus a single-port catheter in ex vivo porcine brain tissue. *J. Eng. Sci. Med. Diag. Ther.* 4, 011003.
- Hayn, L., Deppermann, L., Koch, M., 2017. Reduction of the foreign body response and neuroprotection by apyrase and minocycline in chronic cannula implantation in the rat brain. *Clin. Exp. Pharmacol. Physiol.* 44, 313–323.
- Henstock, J.R., Canham, L.T., Anderson, S.I., 2015. Silicon: the evolution of its use in biomaterials. *Acta Biomater.* 11, 17–26.
- Hood, R.L., Andriani, R.T., Emch, S., Robertson, J.L., Rylander, C.G., Rossmeisl Jr., J.H., 2013a. Fiberoptic microneedle device facilitates volumetric infusate dispersion during convection-enhanced delivery in the brain. *Lasers Surg. Med.* 45, 418–426.
- Hood, R.L., Rossmeisl Jr., J.H., Andriani, R.T., Wilkinson, A.R., Robertson, J.L., Rylander, C.G., 2013b. Intracranial hyperthermia through local photothermal heating with a fiberoptic microneedle device. *Lasers Surg. Med.* 45, 167–174.
- Krauze, M.T., Saito, R., Noble, C., Tamas, M., Bringas, J., Park, J.W., Berger, M.S., Bankiewicz, K., 2005. Reflux-free cannula for convection-enhanced high-speed delivery of therapeutic agents. *J. Neurosurg.* 103, 923–929.
- Linsmeier, C.E., Prinz, C.N., Petterson, L.M., Caroff, P., Samuelson, L., Schouenborg, J., Montelius, L., Danielsen, N., 2009. Nanowire biocompatibility in the brain - looking for a needle in a 3D stack. *Nano Lett.* 9, 4184–4190.
- Liu, Y., Cho, C.W., Yan, X., Henthorn, T.K., Lillehei, K.O., Cobb, W.N., Hg, K.Y., 2001. Ultrasound-induced hyperthermia increases cellular uptake and cytotoxicity of P-glycoprotein substrates in multi-drug resistant cells. *Pharm. Res.* 18, 1255–1261.
- Mehta, A.M., Sonabend, A.M., Bruce, J.N., 2017. Convection-enhanced delivery. *Neurotherapeutics.* 14, 358–371.
- Montagni, E., Resta, F., Mascaro, A.L.M., Pavone, F.S., 2019. Optogenetics in brain research: from a strategy to investigate physiologic function to a therapeutic tool. *Photonics* 6, 92.
- Raghavan, R., Brady, M.L., Rodriguez-Ponce, M.I., Hartlep, A., Pedain, C., Sampson, J.H., 2006. Convection-enhanced delivery of therapeutics for brain disease, and its optimization. *Neurosurg. Focus.* 20, E12.
- Rossmeisl, J., 2017. Maximizing local access to therapeutic deliveries in glioblastoma. Part V: clinically relevant model for testing new therapeutic approaches. In: De Vleeschouwer, S. (Ed.), *Glioblastoma*. Codon Publications, Brisbane, pp. 405–425.
- Rossmeisl, J.H., Herpai, D., Quigley, M., Cecere, T.E., Robertson, J.L., D'Agostino, R.B., Hinckley, J., Tatter, S.B., Dickinson, P.J., Debinski, W., 2021. Phase I trial of convection-enhanced delivery of IL13RA2 and EPHA2 receptor targeted cytotoxins in dogs with spontaneous intracranial gliomas. *Neuro-Oncology* 23, 422–434.
- Saad, A.H., Hahn, G.M., 1992. Ultrasound-enhanced effects of adriamycin against murine tumors. *Ultrasound Med. Biol.* 18, 715–723.
- Sampson, J.H., Archer, G., Pedain, C., Wembacher-Schroder, E., Westphal, M., Kunwar, S., Vogelbaum, M.A., Coan, A., Herndon II, J.E., Raghavan, R., Brady, M.L., Reardon, D.A., Friedman, A.H., Friedman, H.S., Rodriguez-Ponce, M.I., Mittermeyer, S., Croteau, D., Puri, R.K., et al., 2010. Poor drug distribution as a possible explanation for the results of the PRECISE trial. *J. Neurosurg.* 113, 301–309.
- Sharma, P., Sonawane, P., Herpai, D., D'Agostino, R., Rossmeisl, J., Tatter, S., Debinski, W., 2020. Multireceptor targeting of glioblastoma. *Neurooncol. Adv.* 2, vdaa107.
- Ung, T.H., Malone, H., Cannoll, P., Bruce, J.N., 2015. Convection-enhanced delivery for glioblastoma: targeted delivery of antitumor therapeutics. *CNS Oncol.* 4, 225–234.
- Vogelbaum, M.A., Aghi, M.K., 2015. Convection-enhanced delivery for the treatment of glioblastoma. *Neuro-Oncology Suppl* 2, ii3–ii8.
- Vogelbaum, M.A., Brewer, C., Barnett, G.H., Mohammadi, A.M., Peereboom, D.M., Ahluwalia, M.S., Gao, S., 2019. First-in-human evaluation of the Cleveland multiport catheter for convection-enhanced delivery of topotecan in recurrent high-grade glioma: results of pilot trial 1. *J. Neurosurg.* 130, 476–485.
- Zhong, Y., Bellamkonda, R.V., 2008. Biomaterials for the central nervous system. *J. R. Soc. Interface* 5, 957–975.